

RESEARCH

Open Access



Ultrasmall platinum single-atom enzyme alleviates oxidative stress and macrophage polarization induced by acute kidney ischemia–reperfusion injury through inhibition of cell death storm

Keng Ye^{1,2,3}, Kongwen Lin^{1,2,3}, Chengkun Wu⁴, Zhenhuan Zou^{1,2,3}, Yang Zhu^{5,6*} and Yanfang Xu^{1,2,3*}

Abstract

Acute kidney injury (AKI), characterized by a rapid decline in renal function, is associated with impaired mitochondrial function and excessive reactive oxygen species (ROS). Therefore, the exploration of ROS scavengers provides promising new opportunities for the prevention and treatment of AKI by mitigating oxidative stress. Here, we construct an ultrasmall platinum single-atom enzyme (Pt/SAE) with multiple antioxidant enzyme activities to protect against acute kidney ischemia–reperfusion (I/R) injury. Pt/SAE not only mimics superoxide dismutase and catalase activities to convert superoxide anion into water and oxygen, but also exhibits impressive hydroxyl radical scavenging capacity, thereby reducing pro-inflammatory macrophage levels and preventing inflammation. Furthermore, Pt/SAE reduces the accumulation of Z-form DNA, which excessively accumulates following I/R damage, thus decreasing its interaction with Z-DNA binding protein 1, consequently preventing the progression of PANoptosis following I/R stress. Additionally, the downregulation of ROS levels induced by Pt/SAE suppresses lipid peroxidation, which in return preventing the progression of ferroptosis following I/R. Both in vitro and in vivo experiments confirm that Pt/SAE effectively mitigates inflammatory cell infiltration and promotes a shift in macrophage polarization from the M1-like to M2-like subtype. This study provides promising information for the development of novel SAEs as a viable treatment method for AKI.

Keywords Acute kidney ischemia–reperfusion injury, Single-atom enzyme, Ferroptosis, PANoptosis, Macrophages polarization

*Correspondence:

Yang Zhu

zhuyang@mail.ustc.edu.cn

Yanfang Xu

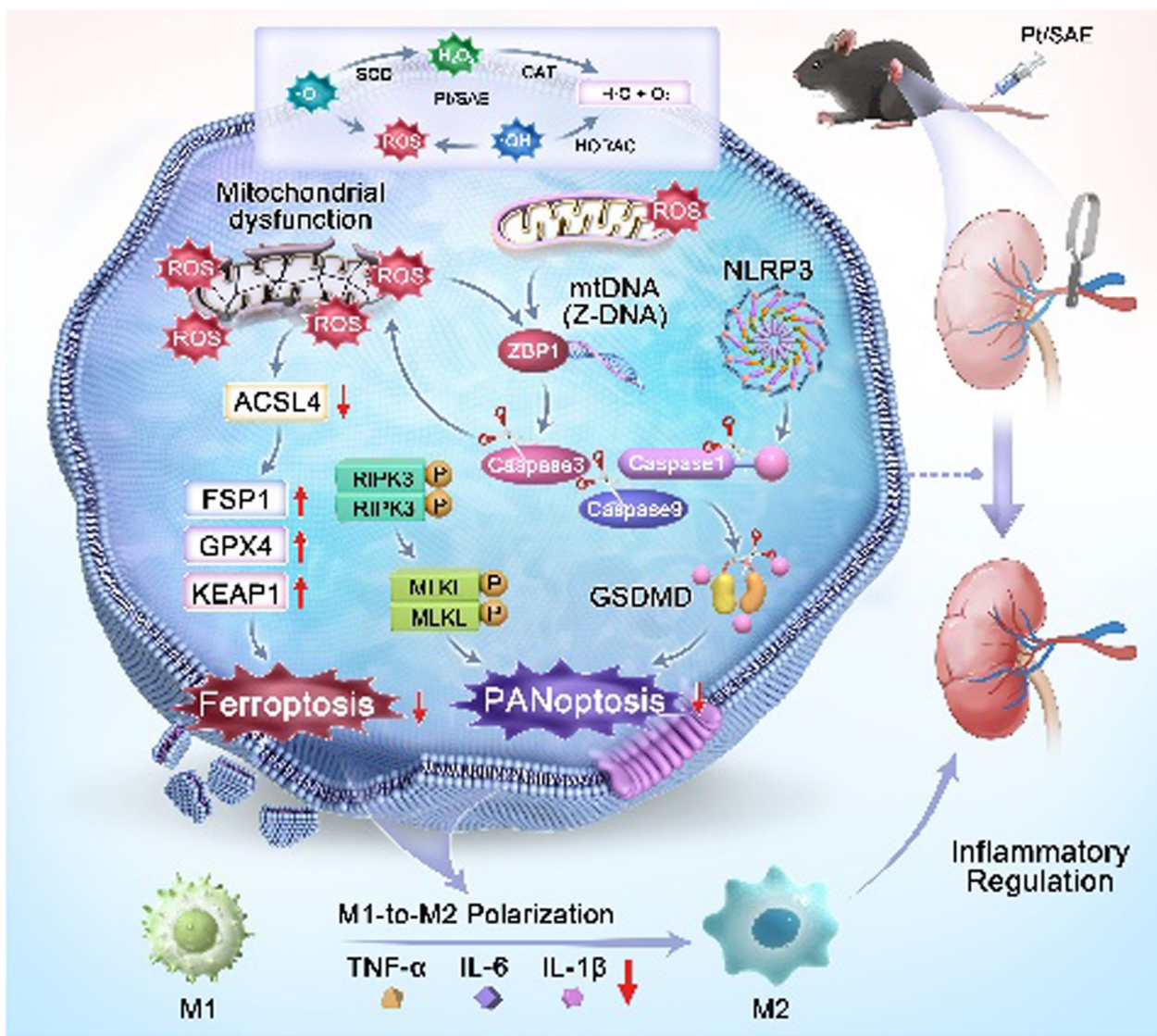
xuyanfang99@hotmail.com

Full list of author information is available at the end of the article



© The Author(s) 2025. **Open Access** This article is licensed under a Creative Commons Attribution-NonCommercial-NoDerivatives 4.0 International License, which permits any non-commercial use, sharing, distribution and reproduction in any medium or format, as long as you give appropriate credit to the original author(s) and the source, provide a link to the Creative Commons licence, and indicate if you modified the licensed material. You do not have permission under this licence to share adapted material derived from this article or parts of it. The images or other third party material in this article are included in the article's Creative Commons licence, unless indicated otherwise in a credit line to the material. If material is not included in the article's Creative Commons licence and your intended use is not permitted by statutory regulation or exceeds the permitted use, you will need to obtain permission directly from the copyright holder. To view a copy of this licence, visit <http://creativecommons.org/licenses/by-nc-nd/4.0/>.

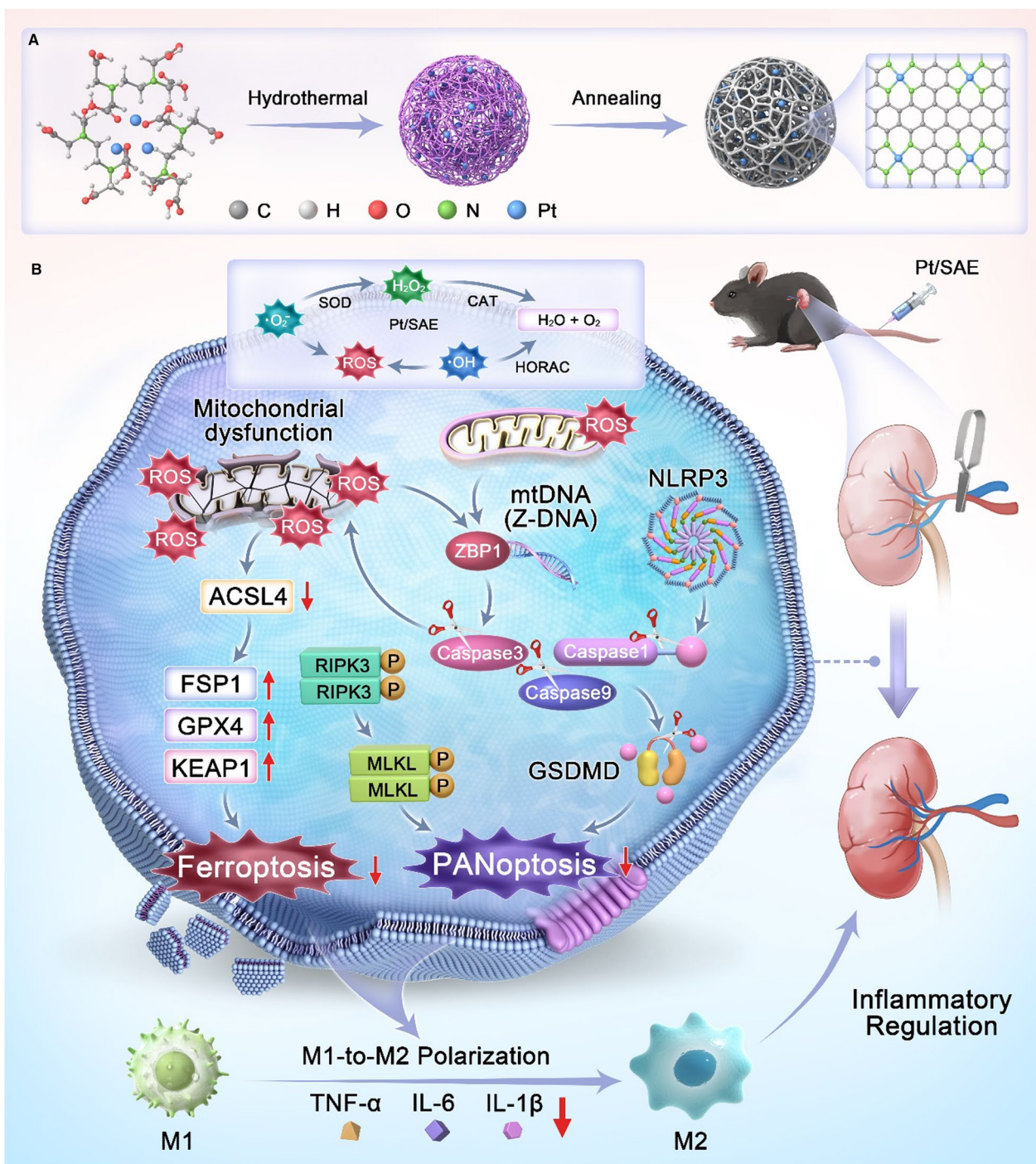
Graphical abstract



Introduction

Acute kidney injury (AKI) is characterized by an abrupt and quick impairment of renal function, which increases the risk of developing chronic kidney disease (CKD), a condition associated with high morbidity and mortality [1–3]. The underlying mechanism remain poorly understood, and there is currently a lack of effective pharmacological therapies that can precisely improve renal function after AKI. AKI is mostly caused by renal ischemia/reperfusion (I/R) injury. Our single-cell sequencing revealed that different regulatory cell death modes are present in IRI, and blocking one kind of cell death alone does not

completely block severe IRI. This indicates the existence of cell death storm in IRI. Acute kidney I/R injury is accompanied by an insufficient oxygen supply and excessive reactive oxygen species (ROS) [4–6]. Mitochondrial ROS is well known to trigger a cascade of events, including mitochondrial dysfunction and the subsequent release of mitochondrial DNA (mtDNA) into the cytoplasm [7–9]. Compelling evidence has established a link between mtDNA instability, which might facilitate the change from B- to Z-DNA structures, mitochondrial dysfunction [10], and cell death storm, including ferroptosis and PANoptosis [11]. Furthermore, ROS-mediated



Scheme 1 Schematic illustrating of the fabrication and application of Pt/SAEs. **A** Schematic depicting the construction of Pt/SAEs. **B** Schematic demonstrating the application of Pt/SAE for the treatment of acute kidney ischemia-reperfusion injury through inhibition of PANoptosis and ferroptosis

ferroptosis or PANoptosis is closely associated with the transformation of microglia to an M1-like phenotype and the generation of inflammatory factors, thus inducing a harmful feedback loop [12–15]. Thus, antioxidant

molecules, including glutathione (GSH) and enzymes such as catalase (CAT) and superoxide dismutase (SOD), represent potential therapeutic options for acute kidney I/R injury [16–18]. Unfortunately, treatments based on

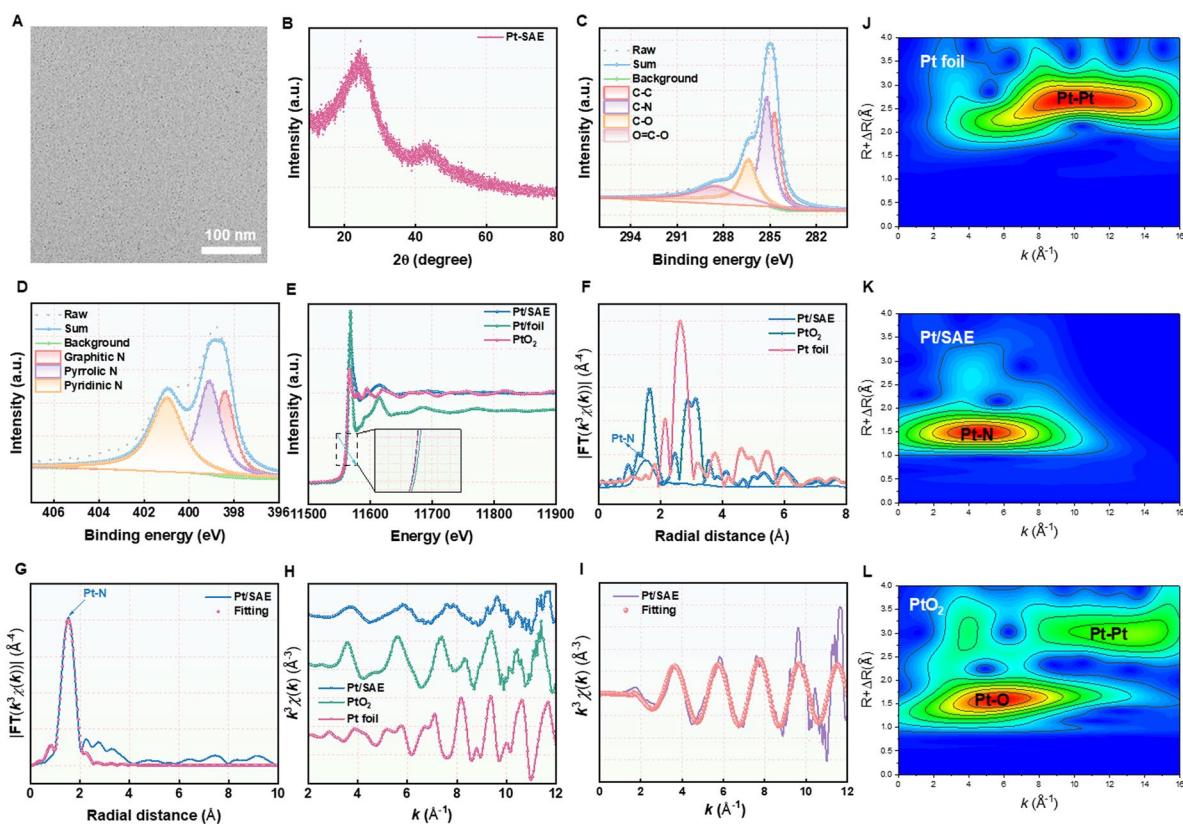


Fig. 1 Comprehensive characterization of Pt/SAE. **A** TEM image of Pt/SAE. **B** XRD spectrum of Pt/SAE. **C** The high-resolution C 1s and **D** N 1s XPS spectra of Pt/SAE. **E** Normalized Pt K-edge XANES spectra of Pt/SAE (inset: the enlarged pre-edge region). **F** The Fourier transform EXAFS of the Pt K-edge of Pt/SAE. **G** EXAFS fitting curve of Pt/SAE at the R space. **H** EXAFS curves of Pt/SAE at the k space. **I** EXAFS fitting curves of Pt/SAE at the k space. **J** Wavelet transformation of Pt K-edge EXAFS of Pt foil, **K** Pt/SAE, and **L** PtO₂ at the k space

these natural enzymes often fail to meet clinical demands due to inherent limitations, including low stability, high cost, and limited membrane permeability [19, 20]. Thus, it is essential to develop novel antioxidant enzyme-mediated catalytic therapeutic strategies to address acute kidney I/R injury.

With the rapid advancement of nanotechnology, nanomedicines have revolutionized the pharmaceutical and biotechnology industries, leading to substantial progress in the development of antioxidant therapies [21–23]. Nanozymes, a class of nanomaterials, demonstrate catalytic activities similar to natural enzymes and have unveiled opened novel avenues for addressing ROS-mediated diseases [9, 24–26]. Nanozymes are emerging as highly promising agents for modulating antioxidant and anti-inflammatory responses, owing to their lower cost, enhanced stability and higher membrane permeability compared to natural enzymes [27–30]. Strong evidence has demonstrated that different nanozymes exhibiting CAT- and SOD-like activities have proven effective in treating AKI by neutralizing harmful ROS, thereby facilitating the recovery of kidney function

[31–34]. While the potential of nanozymes for treating AKI is promising, several challenges persist [35]. First, their relatively low catalytic activities limited their effectiveness in treating acute kidney I/R injury. Second, the relatively large diameters of various nanozymes significantly hindered their effective accumulation in the kidneys [36, 37]. Fortunately, as a next-generation class of nanozymes, single atom enzymes (SAEs), characterized by maximum atom utilization efficacy, well-defined electronic/geometric structures and maximum atom utilization efficacy, bridge the gap between artificial enzymes and nature enzymes, enhancing both intrinsic catalytic activity and substrate selectivity [38–42]. Despite these promising developments, to the best of our knowledge, no reports have yet been published regarding the enzymatic activity of SAEs in acute kidney I/R injury.

Herein, we present an ultrasmall platinum (Pt)/SAE featuring Pt-N₄ active sites anchored on large-surface carbon dots (CDs), designed to effectively alleviate acute kidney I/R injury through scavenging excessive ROS. Pt/SAE not only mimicked the activities of SOD and CAT to convert toxic superoxide anion ($\cdot\text{O}_2^-$) into nontoxic water

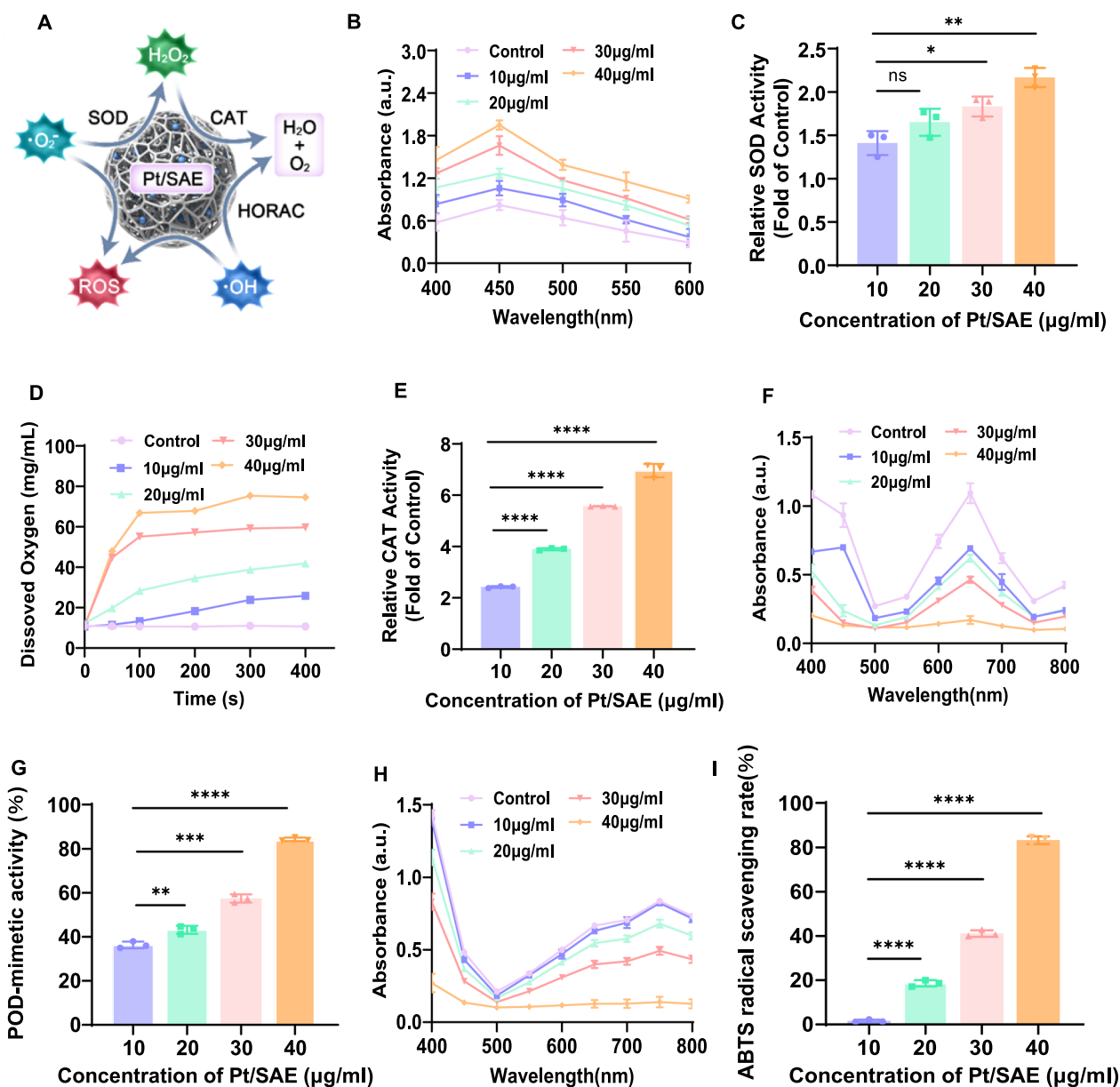


Fig. 2 Enzymatic activity characterization of Pt/SAE. **A** Schematic illustration of multiple enzyme-mimetic activities of Pt/SAE. **B** Quantitative assessment of SOD-like activity. **C** Spectrophotometric comparison of SOD-mimetic activity of different concentrations of Pt/SAE at 450 nm. **D** Quantitative evaluation of CAT-mimetic activity. **E** Comparative analysis of CAT-mimetic activity among different concentrations of Pt/SAE. **F** Quantitative assessment of HORAC. **G** Comparative analysis of HORAC among different concentrations of Pt/SAE. **H** Quantitative assessment of radical-scavenging activity. **I** Spectrophotometric comparison of ABTS radical-scavenging activity of different concentrations of Pt/SAE at 750 nm. n = 3. p-values are calculated using the Student's two-tailed t-test, ns: no significance, * $p < 0.05$, ** $p < 0.01$, *** $p < 0.001$, **** $p < 0.0001$

and oxygen, but also demonstrated excellent hydroxyl radical ($\cdot OH$) scavenging capacity (HORAC), thus inhibiting inflammation. Following cellular uptake, Pt/SAE effectively preserved the mitochondrial function and significantly reduced the accumulation of Z-form DNA, which in return diminished its interaction with Z-DNA binding protein 1 (ZBP1), consequently preventing the

progression of PANoptosis following I/R stress. Furthermore, the reduction of ROS levels induced by Pt/SAE significantly inhibited the lipid peroxidation, thereby preventing the progression of ferroptosis following I/R. In addition, fluorescence imaging revealed that indocyanine green-labeled ultrasmall Pt/SAE effectively accumulated in the kidneys and maintained a high concentration up to

24 h post-injection. Both in vitro and in vivo experiments demonstrated that the inhibitory effects of Pt/SAE on cell death storm effectively reprogram macrophages, attenuate inflammatory cell infiltration, and inhibit macrophage polarization. This study not only provided a proof-of-concept for the exploration of novel SAEs but also offered new insights into nanomedicine for the treatment of acute kidney I/R injury.

Results

Preparation and characterization of Pt/SAE

We synthesized the Pt/SAE with atomically dispersed Pt active sites on CDs through a straightforward pyrolysis of a coordinated complex precursor (Scheme 1A). The Pt-EDTA complex precursor was first prepared via liquid-phase coordination of K_2PtCl_6 with ethylenediaminetetraacetic acid (EDTA). Subsequently, Pt/SAE was obtained by annealing a mixture of the Pt-EDTA complex and Na_2 (EDTA) under an argon atmosphere for 3 h at 300 °C. Transmission electron microscopy (TEM) confirmed that the size of Pt/SAE was consistent, measuring 2–4 nm, a size range typical for SAE (Fig. 1A). The corresponding powder X-ray diffraction (XRD) pattern exhibited no crystalline peaks attributable to metallic Pt or Pt oxide nanoparticles, indicating the absence of notable Pt aggregation, which supports the formation of atomically dispersed Pt sites (Fig. 1B). Raman spectroscopy revealed that the CDs were poorly crystallized post-pyrolysis and contained a significant number of defects, which likely facilitates the anchoring of isolated Pt atoms (Figure S1). X-ray photoelectron spectroscopy (XPS) analysis was conducted to investigate the bonding states of Pt, C, and N atoms in Pt/SAEs. The high-resolution C 1s spectrum primarily exhibited peaks associated with sp^2 -hybridized graphitic carbon (Figs. 1C and S2). The high-resolution N 1s spectrum displayed three distinct species: graphitic N, pyridinic N, and pyrrolic N, all of which contribute to anchoring the single-atomic Pt species (Fig. 1D). To further explore the coordination environment and local electronic structure of Pt, synchrotron radiation-based X-ray absorption near-edge structure (XANES) analysis was performed. The Pt K-edge XANES spectra revealed an energy absorption threshold between

that of Pt foil and PtO_2 (Fig. 1E), suggesting that the Pt atoms in Pt/SAEs possess an oxidation state of $Pt\delta^+$ ($0 < \delta < 4$), which aligns with the XPS findings. Additionally, Fourier-transform extended X-ray absorption fine structure (EXAFS) analysis in the R-space domain showed a prominent peak at 1.53 Å, corresponding to the Pt–N bond, while no peaks were observed at 2.64 Å, which would be indicative of Pt–Pt bonding. This result confirms the presence of atomically dispersed Pt active sites within Pt/SAE (Figs. 1F, G and S3). EXAFS fitting analysis at the Pt K-edge provided detailed information on the coordination numbers and structural parameters of the single-atomic Pt species. As shown in Figs. 1H, I, S4, and Table S1, the analysis revealed that each Pt atom in Pt/SAE is coordinated with approximately four N atoms. To further substantiate the atomic dispersion of Pt, wavelet transform (WT) analysis was performed. As expected, a WT signal at 4.5 Å⁻¹, corresponding to the Pt–N bond, was observed, while no signal indicative of Pt–Pt bonding was detected (Fig. 1J–L). We have investigated the stability of Pt/SAE in DMEM and blood sample. As shown in Figure S5 the DLS result showed that the diameter of Pt/SAE remained stable for 96 h, which indicated the stability of Pt/SAE in DMEM and blood sample. These collective findings unequivocally demonstrate the successful construction of Pt/SAEs with atomically dispersed Pt–N₄ sites.

Enzymatic performances of Pt/SAE in PTECs

Following the characterization of the coordination environment of Pt atoms in Pt/SAE, we systematically investigated the dual reactive oxygen species (ROS) scavenging activities of Pt/SAE. The enzymatic properties of Pt/SAE were assessed to validate its ROS-scavenging capacity (Fig. 2A). To evaluate the superoxide dismutase (SOD)-mimetic activity, we employed the WST-8 assay. Pt/SAE demonstrated excellent concentration-dependent SOD-like catalytic performance. Comparative analysis (Fig. 2B, C) revealed that Pt/SAE exhibited superior catalytic efficiency relative to other systems. Furthermore, we assessed the catalase (CAT)-like activity of Pt/SAE using a dissolved oxygen analyzer (Fig. 2D–E). The results demonstrated that Pt/

(See figure on next page.)

Fig. 3 Cellular uptake, viability, and protective effects of Pt/SAE. **A** CLSM images illustrated time-dependent cellular uptake of Cy5-labeled Pt/SAE. Nuclei were stained with Hoechst for visualization. Scale bar = 40 μm. **B** Cy5-labeled Pt/SAE colocalized with lysosomes, demonstrating its potential to escape from lysosomes into the cytoplasm. Scale bar = 25 μm. **C** The CCK-8 assay was used to examine dose-dependent cell viability in PTECs exposed to various concentrations of Pt/SAE. **D, E** Fluorescence microscopy showed the cellular protection of Pt/SAE in PTECs following H/R, with Annexin V and PI staining to assess apoptosis and necrosis. Scale bar = 25 μm. **F** The cellular protection of Pt/SAE in PTECs following H/R was determined by flow cytometry with Annexin V and PI staining. n = 5. **G** Intracellular ROS production after different treatments was assessed by CLSM. Scale bar = 20 μm. **H** Intracellular ROS generation following various treatments was examined by flow cytometric analysis. *p*-values are calculated using the Student's two-tailed *t*-test, ****p* < 0.001, *****p* < 0.0001

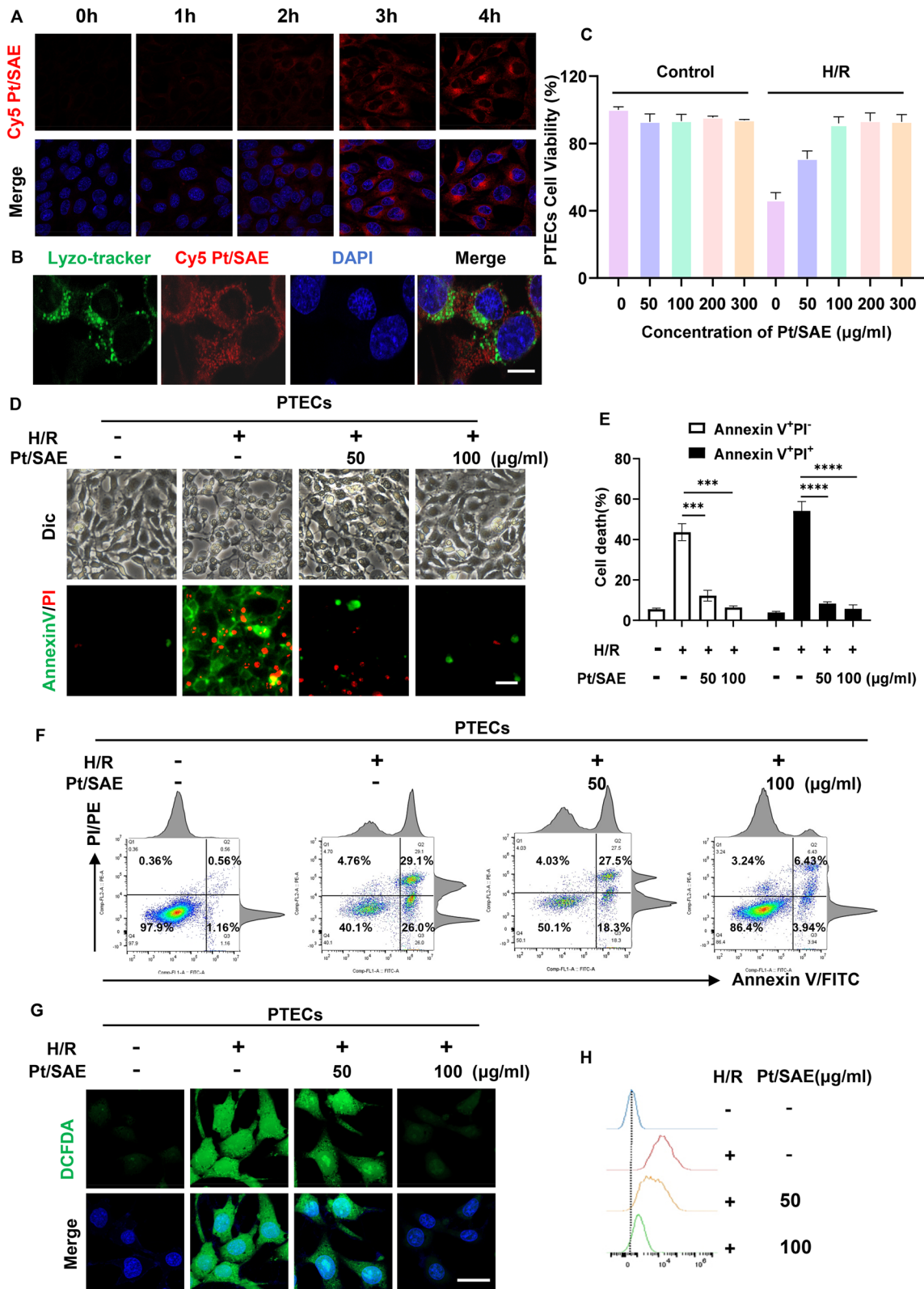


Fig. 3 (See legend on previous page.)

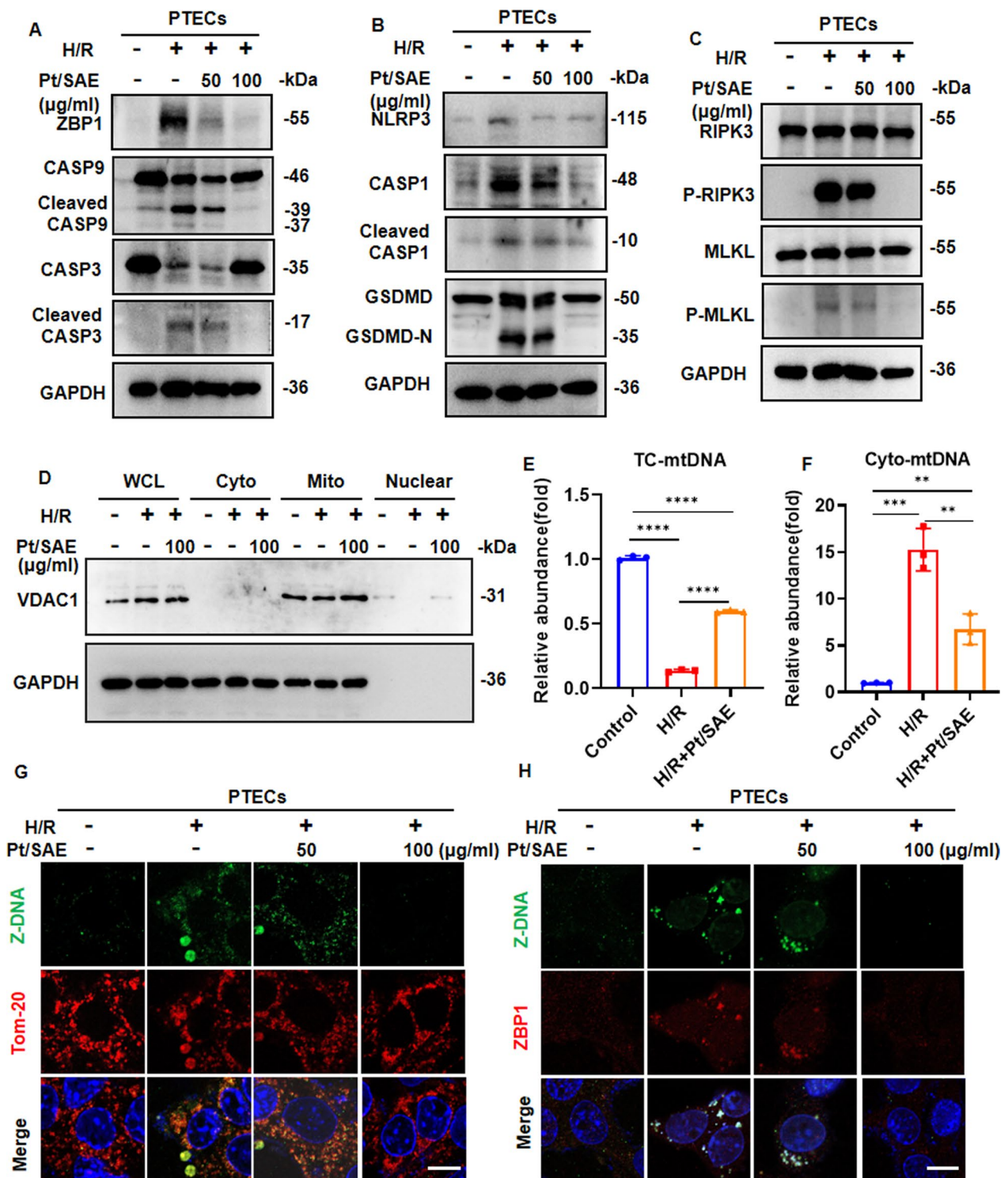


Fig. 4 Pt/SAE Significantly Alleviates H/R-Induced PANoptosis and Z-mtDNA formation. **A–C** Representative immunoblots of PANoptosis-related proteins in PTECs. *n* = 3. **D** Cellular fractionation was performed to acquire pure mitochondrial fractions. GAPDH = cytoplasm marker. VDAC1 = mitochondrial marker. **E, F** QPCR was used to quantify the amounts of cytosolic mitochondrial DNA (Cyto-mtDNA) and total cellular mitochondrial DNA (TC-mtDNA) in PTECs treated with Pt/SAE followed by H/R stimulation. **G** Colocalization of Z-DNA and mitochondria was shown by staining for DAPI (nuclei) and Tom-20 (mitochondrial marker). **H** Z-DNA induced by H/R was sensed and colocalized with ZBP1. Nuclei were stained with DAPI. Scale bar = 10 µm. *p*-values are calculated using the Student's two-tailed *t*-test, **p* < 0.05, ***p* < 0.01, ****p* < 0.001, *****p* < 0.0001

SAE effectively catalyzed the decomposition of H_2O_2 into water and oxygen, thereby mitigating ROS-induced oxidative stress. Additionally, as illustrated in Fig. 2F, G, Pt/SAE displayed effective hydroxyl radical ($\cdot OH$) scavenging activity in the HORAC assay. Pt/SAE also exhibited remarkable ABTS radical scavenging capability (Fig. 2H, I). Collectively, these findings underscore the impressive ROS-scavenging capacity of Pt/SAE.

The cellular uptake of Cy5-labeled Pt/SAE was visualized using laser confocal scanning microscopy. Fluorescence intensity analysis revealed time-dependent internalization of Pt/SAE in mouse primary proximal tubular epithelial cells (PTECs) (Fig. 3A). Colocalization studies demonstrated that Cy5-labeled Pt/SAE could effectively escape from the lysosomes into the cytoplasm, subsequently leading to ROS consumption (Fig. 3B). Biocompatibility was assessed using the cell counting kit-8 (CCK-8) assay, demonstrating negligible inhibition of PTEC proliferation, even at concentrations up to 300 $\mu g/mL$ (Fig. 3C). To explore the protective effects of Pt/SAE against oxidative stress, an in vitro ischemia–reperfusion injury (IRI) model was established by subjecting PTECs to hypoxia/reoxygenation (H/R) stress. Pt/SAE significantly enhanced cell viability following exposure to hypoxia/reoxygenation (H/R) stress, suggesting its potent properties on protecting against oxidative stress induced damage. Additionally, the protective efficacy of Pt/SAE was evaluated by flow cytometry and fluorescence microscope using Annexin V and PI staining. Quantification of double-positive (Annexin V +/PI +) PTECs revealed that Pt/SAE treatment significantly reduced the proportion of apoptotic/necrotic cells after H/R stimulation, exhibiting a dose-dependent protective effect, which was consistent with the results of the CCK-8 assay (Fig. 3D–F and S16). We evaluated the cellular antioxidant capacity of Pt/SAE in H/R-induced oxidative stress. The ROS-sensitive dye dichlorodihydrofluorescein diacetate (DCFH-DA) was used to quantify intracellular ROS levels using confocal laser scanning microscopy (CLSM). PTECs exposed to H/R exhibited significantly elevated ROS production. Contrarily, cells treated with Pt/SAE demonstrated a marked reduction in ROS levels, indicating effective ROS scavenging after Pt/SAE treatment in this H/R model

(Fig. 3G). Additionally, flow cytometry analysis using DCFH-DA detected widespread distribution of ROS in the H/R group, indicating aggravated oxidative stress damage within the mitochondria. However, Pt/SAE treatment significantly alleviated this damage (Fig. 3H). These findings provide compelling evidence for the excellent protective capacity of Pt/SAE and its ability to mitigate renal epithelial cell death in IRI models.

Pt/SAE significantly alleviates H/R-induced PANoptosis and Z-mtDNA formation

PANoptosis, a form of programmed cell death associated with by oxidative stress and mitochondrial dysfunction, involves three types of cell death: pyroptosis, apoptosis, and necroptosis. It has been implicated in the pathogenesis of ischemia–reperfusion injury. Intriguingly, apoptosis inhibitor (Z-VAD-FMK, 20 μM), pyroptosis inhibitor (Disulfiram, 2 μM) and necrosis inhibitor (Necrosulfonamide, 10 μM) failed to totally prevent H/R-induced PTECs death (Figure S18), suggesting that the three programmed cell death (PCD) pathways that may be regulated by pan-apoptosis function together. ZBP1, the core protein mediating PANoptosis, plays a critical role in this process. To further investigate the involvement of ZBP1-mediated cell death in PTECs during H/R, we detected the key protein expression levels of ZBP1-mediated cell death. The significantly elevated levels of PANoptosis-related proteins ZBP1, cleaved caspase-3, cleaved caspase-9, cleaved GSDMD, cleaved caspase-1, p-RIPK3 and p-MLKL in the H/R group compared to the control group were also observed, along with the elevated IL-1 β and IL-18. Remarkably, treatment with Pt/SAE significantly reduced the expression of PANoptosis-related proteins and the secretion of inflammatory factors, indicating its inhibitory effect on PANoptosis (Figs. 4A–C, S14 C–H, S15D–K and S17). Given the established link between mitochondrial dysfunction and H/R-induced cell death, we investigated the role of mitochondrial pathways, focusing on mitochondrial DNA (mtDNA). Quantitative PCR analysis revealed a marked decrease in total cellular mtDNA and an increase in cytosolic mtDNA release in the H/R group. Pt/SAE treatment significantly mitigated both effects, suggesting its protective role in

(See figure on next page.)

Fig. 5 Pt/SAE significantly alleviates H/R-induced ferroptosis. **A** JC-10 staining was used to assess the mitochondrial membrane potential (MMP) in H/R-induced PTECs following Pt/SAE therapy. Scale bar = 10 μm . **B** CLSM was used to examine the colocalization of mitochondria and Mito-ROS in PTECs treated with Pt/SAE following H/R. Mito-tracker and MitoSOX probes were used for labeling. Nuclei were stained with Hoechst for visualization. Scale bar = 10 μm . **C** Lipid ROS levels were measured using C11-bodipy probe by CLSM. Scale bar = 10 μm . **D** Representative micrographs of the colocalization of intracellular iron level (FerroOrange staining) and mitochondria (Mito-tracker staining) in PTECs. Nuclei were stained with Hoechst for visualization. Scale bar = 10 μm . **E** Representative immunoblots of ferroptosis-related proteins in PTECs. $n = 3$. **F** Lipid ROS levels were measured using C11-bodipy probe by FACS. p -values are calculated using the Student's two-tailed t -test, * $p < 0.05$, ** $p < 0.01$, *** $p < 0.001$, **** $p < 0.0001$

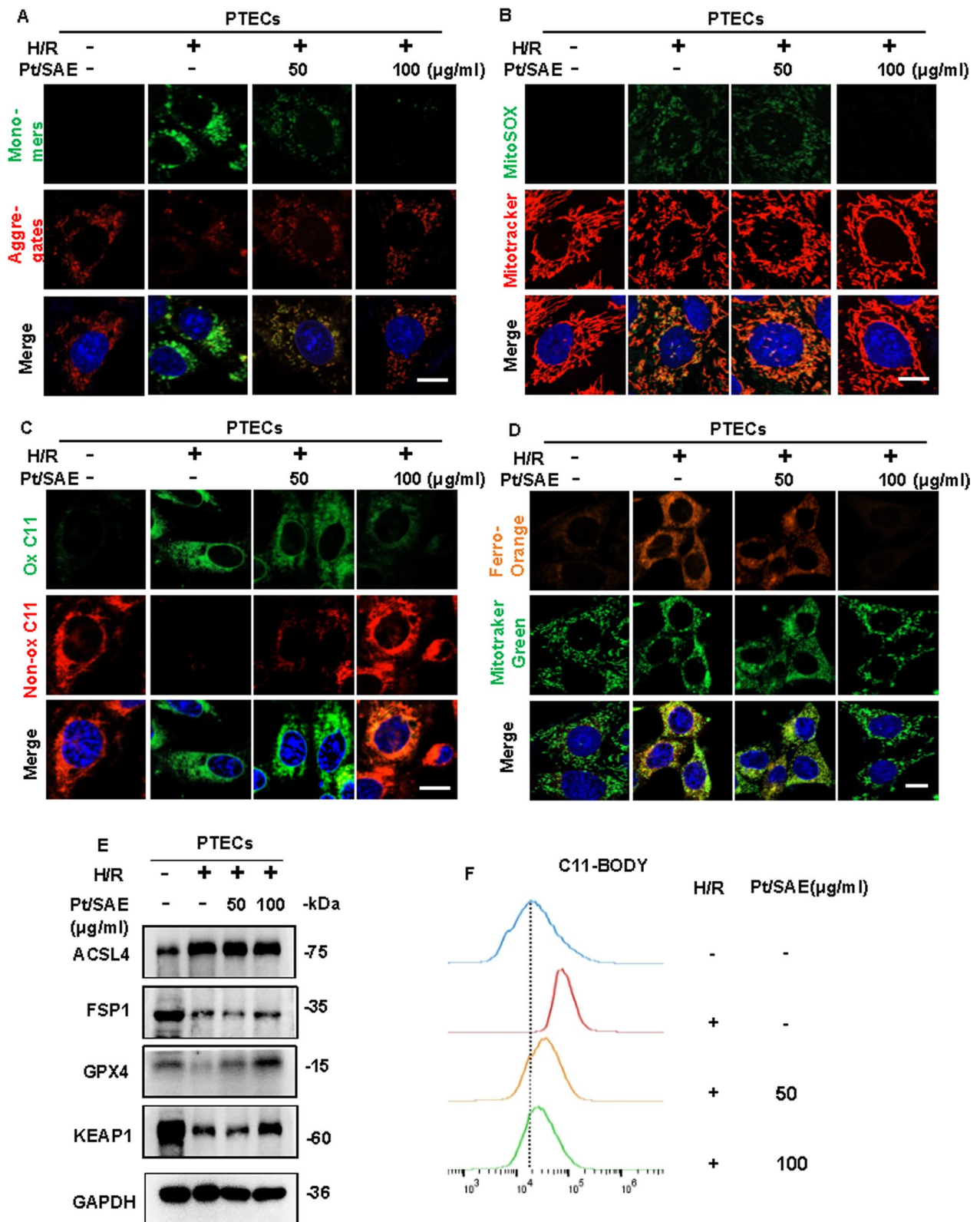


Fig. 5 (See legend on previous page.)

maintaining mitochondrial integrity (Fig. 4D–F). To confirm the occurrence of Z-DNA formation, we performed immunofluorescence staining using a specific anti-Z-DNA antibody. Following H/R treatment, a significant increase in Z-DNA signaling was observed, indicating the synthesis of Z-DNA. Notably, the Z-DNA signal was distinct from nuclear regions, as evidenced by the lack of overlap with DAPI staining. This finding suggests that the release of Z-DNA originates from mitochondria rather than the nucleus. Colocalization studies further revealed that Z-DNA signaling overlapped with the mitochondrial marker Tom-20 (Fig. 4G) and ZBP1 (Fig. 4H), highlighting a close association between Z-DNA, mitochondrial damage, and ZBP1 activation during H/R. These results demonstrate that H/R-induced mitochondrial damage leads to the release of Z-mtDNA, which colocalizes with ZBP1 and contributes to PANoptosis. Pt/SAE effectively attenuates these processes, emphasizing its potential as a therapeutic agent to combat mitochondrial dysfunction and oxidative stress-induced programmed cell death in ischemia–reperfusion injury.

Pt/SAE significantly alleviates H/R-induced ferroptosis

Ferroptosis, a regulated form of cell death driven by the accumulation of lipid peroxides in plasma membranes, has been implicated in conditions such as cancer, neurodegeneration, renal injury, ischemia/reperfusion injury, and immune dysfunction. This process often coincides with mitochondrial damage. To investigate the role of ferroptosis in PTECs under H/R stress, we assessed mitochondrial function and oxidative stress levels. Figure 5A illustrates that excessive ROS accumulation in PTECs during H/R led to mitochondrial membrane depolarization. Pt/SAE treatment mitigated this effect, with reduction in mitochondrial membrane potential (MMP), suggesting that Pt/SAE reduces ROS-induced oxidative stress in PTECs. Changes in mitochondrial morphology and mitochondrial ROS accumulation were further evaluated using Mitotracker and MitoSOX probes (Fig. 5B). Compared to the H/R group, Pt/SAE treatment significantly alleviated mitochondrial fragmentation and reduced oxidative stress markers, indicating improved mitochondrial integrity. To confirm the occurrence of ferroptosis, we measured lipid peroxidation in cellular

membranes using the BODIPY581/591 C11 probe. Confocal laser scanning microscopy (CLSM; Fig. 5C) and flow cytometry (Fig. 5F) showed that oxidized C11 levels were significantly elevated in the H/R group, indicating extensive lipid peroxidation. However, Pt/SAE treatment markedly reduced oxidized C11 levels. Ferro-orange probes were employed to assess Fe²⁺ levels, a key component of ferroptosis, and revealed elevated Fe²⁺ content in H/R PTECs (Fig. 5D). Pt/SAE treatment effectively decreased this elevation, further supporting its protective role against ferroptosis. We also evaluated the expression of ferroptosis-related proteins, including ACSL4, FSP1, GPX4, and KEAP1 (Figs. 5E, S14 A–B and S15 A–C). In the H/R group, GPX4, FSP1, and KEAP1 levels were decreased, while ACSL4 levels were increased, indicating enhanced ferroptosis. Pt/SAE treatment reversed these changes, restoring protein expression to levels comparable to the control group. In summary, these findings demonstrate that H/R stress promotes ferroptosis in PTECs by increasing ROS, lipid peroxidation, mitochondrial dysfunction, and Fe²⁺ accumulation. Pt/SAE effectively suppresses these processes, reducing ferroptosis and improving mitochondrial homeostasis. Together with its inhibition of PANoptosis, Pt/SAE offers a dual protective mechanism against H/R-induced cytotoxicity in PTECs.

Pt/SAE exhibited kidney-targeting abilities

Before assessing therapeutic efficacy, the biosafety of Pt/SAE was evaluated to ensure its suitability. Pt/SAE demonstrated minimal hemolytic activity (< 5%) across concentrations ranging from 0 to 300 µg/mL, supporting its intravenous administration (Figure S6). Blood biochemistry analysis showed no significant alterations in serum creatinine (Scr), blood urea nitrogen (BUN), alanine aminotransferase (ALT), or aspartate aminotransferase (AST) levels (Figures S7–8), indicating no adverse effects on liver or kidney function. Histological examination of major organs (brain, lung, liver, spleen, and kidney) using H&E staining revealed no signs of tissue damage (Figure S9) and routine blood tests showed no significant alterations in hemoglobin, platelet and neutrophils levels (Figure S10), further confirming the excellent biocompatibility of Pt/SAE. To examine the *in vivo* distribution of Pt/SAE, live imaging of small animals was conducted.

(See figure on next page.)

Fig. 6 Pt/SAE significantly alleviates H/R-induced ferroptosis. **A** IVIS imaging system measurement of fluorescence images in the kidneys of mice treated with ICG-labeled Pt/SAE at 2 h, 4 h, 8 h, 12 h and 24 h following injection. *n* = 3. **B** ICG-labeled Pt/SAE biodistribution and quantification in major organs, such as the brain, heart, liver, spleen, and lung, 12 h and 24 h after intravenous treatment. *n* = 3. All images were taken using the same excitation light strength, exposure duration (*t* = 0.2 s), and detection parameters. **C** PAS staining of kidney slices of renal I/R-injured mice after Pt/SAE treatment. Scale bar = 100 µm. **D** TUNEL evaluation of renal tubular apoptosis in renal I/R-injured mice following Pt/SAE treatment. Scale bar = 50 µm. **E** The levels of Scr and BUN in I/R induced mice with Pt/SAE treatment after 24 h. *n* = 3. *p*-values are calculated using the Student's two-tailed *t*-test, **p* < 0.05, ***p* < 0.01, ****p* < 0.001, *****p* < 0.0001

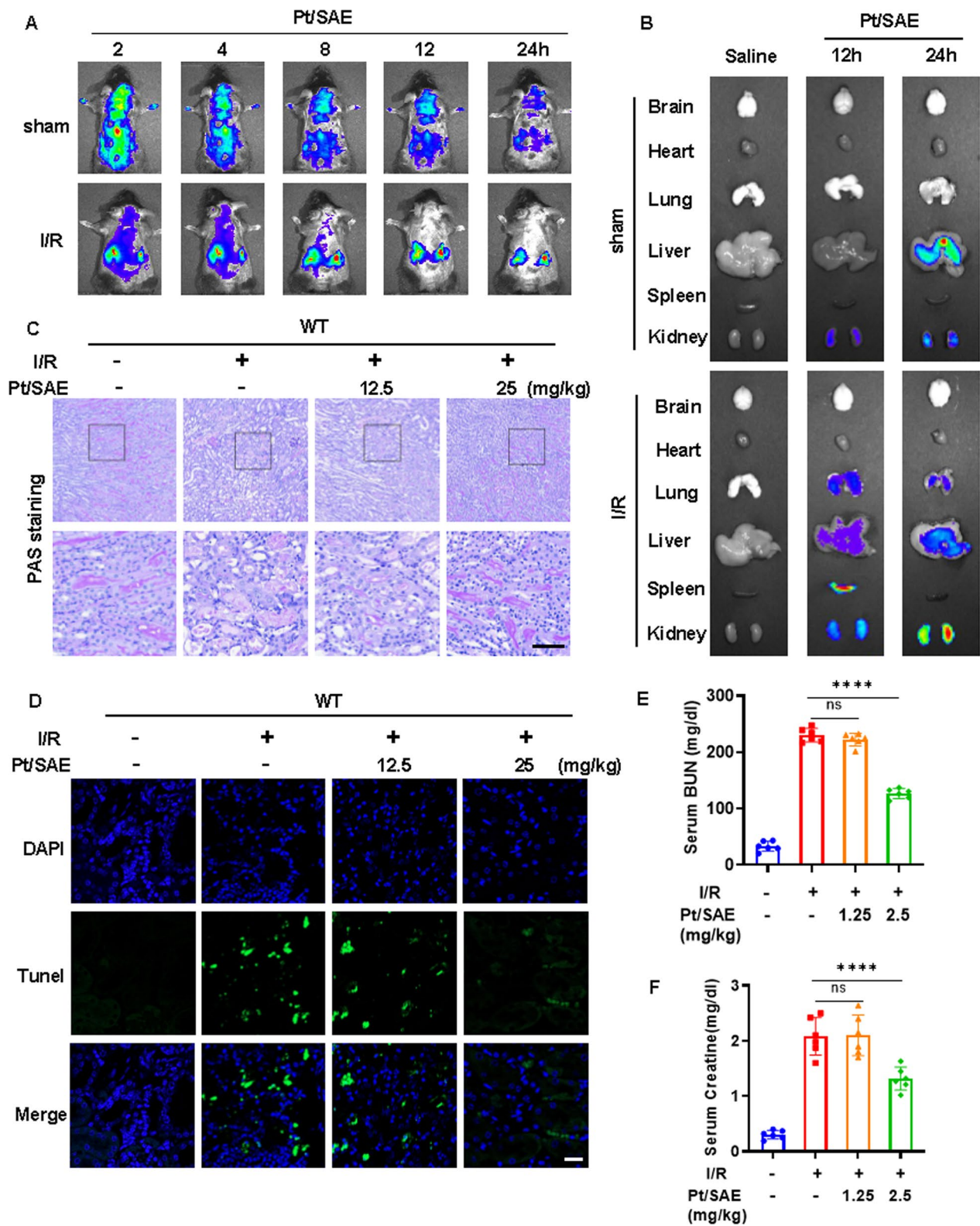


Fig. 6 (See legend on previous page.)

Using a murine renal ischemia/reperfusion injury (IRI) model, where renal pedicles were clamped for 45 min, ICG-labeled Pt/SAE was administered via tail vein injection. Fluorescence imaging (FLI) demonstrated the accumulation of ICG-labeled Pt/SAE in the sham group mice at 2 h after intravenous injection, followed by gradual metabolism over time. Notably, the fluorescence signal at the kidney (targeted organ) after IRI remained robust even at 24 h post-injection, proving the increased accumulation of Pt/SAE in the damaged kidney, which suggested their potential for prolonged therapeutic effects and targeted treatment in acute kidney injury (Fig. 6A, B).

The protective efficacy of Pt/SAE was evaluated in IRI mice. Saline-treated mice exhibited substantial tubular damage, including cellular debris accumulation, epithelial cell detachment, and brush border loss, as observed through Periodic Acid-Schiff (PAS) staining (Fig. 6C and S11). Pt/SAE treatment significantly reduced these injury markers, with a higher dose (2.5 mg/kg) providing more pronounced protection compared to the lower dose (1.25 mg/kg). Cell apoptosis was assessed using TUNEL assays, revealing a marked reduction in TUNEL-positive cells in Pt/SAE-treated renal tissues compared to saline-treated controls (Fig. 6D). Functional improvements were corroborated by a significant reduction in serum creatinine (Scr) and blood urea nitrogen (BUN) levels in Pt/SAE-treated mice. High-dose Pt/SAE treatment (2.5 mg/kg) achieved greater reductions in Scr and BUN levels compared to the low-dose group (1.25 mg/kg) (Fig. 6E, F). In conclusion, Pt/SAE exhibits excellent kidney-targeting capabilities, particularly in injured kidneys, and provides dose-dependent protection against renal ischemia/reperfusion injury. This nanomedicine holds promise for targeted therapy and functional recovery in acute kidney injury.

Pt/SAE ameliorates I/R-induced nephrotoxicity by suppressing ferroptosis and PANoptosis

To gain further insights into the protective effect of Pt/SAE in I/R-induced AKI, a thorough investigation was carried out. Oxidative stress plays a pivotal role on mitochondria as a key mechanism in ferroptosis-mediated kidney injury. 4-HNE, a lipid peroxidation product, was assessed in the renal tissues of mice with I/R-induced

AKI. Following I/R, the kidneys showed noticeably greater levels of oxidative stress injury (Fig. 7A). We further confirmed oxidative stress and ferroptosis-related protein expression in the proximal tubules isolated from kidney tissues further confirming the therapeutic efficacy of Pt/SAE in inducing renal oxidative stress. Mice with I/R-induced AKI showed reduced expression of GPX4 and FSP1 and increased expression of the core ferroptosis protein ACSL4. I/R-induced tubular damage resulted in a reduction in the expression of the oxidative stress-related protein KEAP-1 and were like those from in vitro studies (Figs. 7B, S12 A, B and S13 A–C). The immunofluorescence of renal tissue also showed that Pt/SAE could alleviate the reduction of GPX4 in the I/R mouse models (Fig. 7C). According to our research, the groups treated with Pt/SAE also showed lower expression of the apoptosis markers cleaved caspase-3 and cleaved caspase-9, PANoptosis core response protein Z-DNA-binding protein 1 (ZBP1), necroptosis marker p-MLKL, and pyroptosis marker cleaved GSDMD than the I/R group (Figs. 7D–F, S12 C–H and S13D–K). The western blot method showed similar results to those from the in vitro study and was also detected in kidney tissues. Cytosolic Z-DNA was found to colocalize with ZBP1 in renal tubules after I/R. The colocalization phenomenon was significantly reduced after Pt/SAE administration (Fig. 7G). These findings indicated that Pt/SAE can prevent I/R-induced PANoptosis.

Pt/SAE attenuates inflammatory cell infiltration and inhibited macrophages polarization

Inflammatory cells play a critical role in the pathogenesis of kidney injury. To assess the extent of inflammatory cell infiltration, we employed Ly6G (Fig. 8A) and F4/80 (Fig. 8B) as specific markers for neutrophils and monocytes/macrophages, respectively. Immunofluorescence staining revealed a significant increase in inflammatory cell infiltration following I/R injury. However, treatment with Pt/SAE markedly reduced the infiltration of both neutrophils and monocytes/macrophages, highlighting its protective effect in modulating the inflammatory response during kidney injury. Macrophage polarization is a key determinant in the progression and resolution of renal damage, inflammation, and fibrosis. Macrophages are categorized into two phenotypes: pro-inflammatory

(See figure on next page.)

Fig. 7 Pt/SAE ameliorates I/R-Induced Nephrotoxicity by suppressing ferroptosis and PANoptosis. **A** Immunofluorescence staining of 4-HNE (red), Megalin (green) and DAPI (blue) in kidneys after I/R with Pt/SAE. Scale bar = 50 μ m. **B** Representative immunoblots of ferroptosis-related proteins in kidney tissues. n = 3. **C** Immunofluorescence staining of GPX4 (red), Megalin (green) and DAPI (blue) in kidneys after I/R with Pt/SAE. Scale bar = 50 μ m. **D–F** Representative immunoblots of PANoptosis-related proteins in kidney tissues. n = 3. **G** Immunofluorescence staining of ZBP1 (red), Z-DNA (green) and DAPI (blue) in kidneys after I/R with Pt/SAE. Scale bar = 50 μ m. *p*-values are calculated using the Student's two-tailed *t*-test, **p* < 0.05, ***p* < 0.01, ****p* < 0.001, *****p* < 0.0001

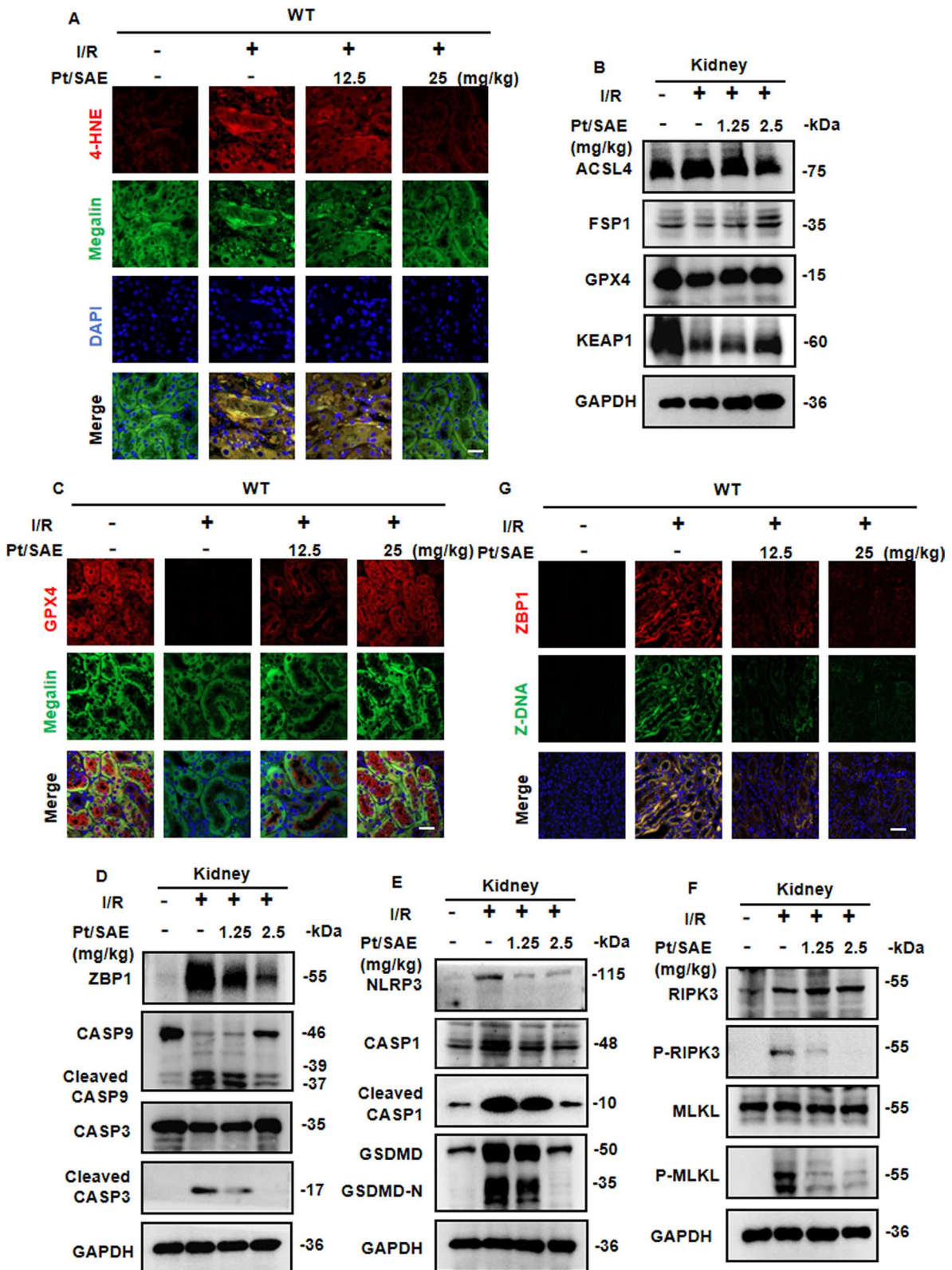


Fig. 7 (See legend on previous page.)

M1 macrophages, which exacerbate tissue damage, and anti-inflammatory M2 macrophages, which promote tissue repair. To investigate the impact of Pt/SAE on macrophage polarization, flow cytometry analysis was conducted on kidney tissues. The results demonstrated a substantial increase in iNOS + cells (M1 macrophages) following I/R injury, which was significantly attenuated by Pt/SAE treatment. Similarly, CD206 + cells (M2 macrophages) were increased following I/R injury, and Pt/SAE treatment partially reduced their presence (Fig. 8C–F). The role of pro-inflammatory cytokines in renal damage was further evaluated by measuring TNF- α , IL-1 β , and IL-6 levels in kidney tissues. These cytokines were significantly elevated in response to I/R injury, consistent with a strong inflammatory response (Fig. 8G–I). Pt/SAE treatment, however, markedly reduced the levels of these pro-inflammatory cytokines, indicating its efficacy in suppressing renal inflammation. The inflammatory response of BMDMs was also assessed in a coculture system with H/R-induced PTECs (Fig. 9A). Flow cytometry analysis demonstrated a similar trend to the *in vivo* results, with Pt/SAE effectively inhibiting macrophage polarization (Fig. 9B–D). Additionally, qPCR analysis revealed that the mRNA expression of M1 and M2 macrophage-associated markers was significantly altered following H/R treatment, but Pt/SAE treatment mitigated these changes (Fig. 9E–I). Collectively, these findings suggest that Pt/SAE attenuates inflammatory cell infiltration and suppresses macrophage polarization during I/R injury. This modulation is closely linked to the reduction of the inflammatory response and the prevention of profibrotic processes in the injured kidney.

Discussion

This study introduces a novel antioxidant nanozyme (Pt/SAE) with a single platinum (Pt) atom that significantly mitigates I/R-induced AKI. The designed nanozyme exhibits remarkable enzymatic capabilities for ROS scavenging, characterized by high efficiency, stability, synergistic effects, and metallic electronic properties. It overcomes the inherent limitations of natural antioxidants, such as short circulation time, limited kidney-targeting ability, and poor membrane permeability. Importantly, Pt/SAE demonstrated robust antioxidant properties while reducing inflammation and cell death

storm in renal tissues, including ferroptosis and PANoptosis. These findings suggest a promising therapeutic approach for treating I/R-related kidney injuries. Furthermore, the Pt/SAE demonstrated minimal toxicity, favorable biocompatibility, and safety, providing a strong foundation for potential clinical applications.

Recently our single-cell sequencing indicated that multi-cell death modes (cell death storm) were activated in the cluster of injured PTECs in IRI. PANoptosis, a newly identified form of regulated cell death encompassing pyroptosis, necroptosis, and apoptosis, has emerged as a potential contributor to IRI and organ damage. Although the precise signaling pathways remain undefined, existing evidence suggests that renal IRI induces pyroptosis in tubular epithelial cells. For instance, Katharina Thomas et al. demonstrated that glutamine alleviates kidney injury and enhances renal function in an ischemia/reperfusion injury (IRI)-induced mouse AKI model. Glutamine was shown to promote transcriptomic and proteomic reprogramming in murine renal tubular epithelial cells (TECs), improving mitochondrial function and oxidative phosphorylation while reducing epithelial apoptosis. Research has indicated that tubular and glomerular endothelial cells are more susceptible to necroptosis compared to mesangial cells and podocytes. Elevated expression of RIPK1, RIPK3, and MLKL has been observed in these cells, indicating a predisposition to necroptosis. Western blot analysis has confirmed the presence of RIPK1 and RIPK3 in whole kidney lysates and isolated proximal tubules, with increased MLKL expression following reperfusion. The activation of necroptosis can be further validated by detecting alterations in the phosphorylation state or membrane accumulation of RIPK1, RIPK3, and MLKL through immunoblotting or immunohistochemistry. Investigations using KO mice or specific inhibitors are essential for elucidating the role of necroptosis in renal IRI. Ferroptosis also plays a critical role in the pathophysiology of renal IRI [43]. Linkermann et al. identified its importance, while Xin Gou et al. demonstrated that IRI promotes increased lipid peroxidation and iron levels, decreased GSH levels, and reduced cell viability in normal HK-2 cells [44]. These effects were significantly mitigated when exosome production was inhibited, highlighting the role of IRI exosomes in propagating the “ferroptosis wave.” Further research is needed

(See figure on next page.)

Fig. 8 Pt/SAE provides robust protection against immune inflammation and macrophage polarization during IRI-induced kidney injury. **A, B** Representative images of immunofluorescence staining of macrophage (F4/80 +) and neutrophil (Ly6G +) (red) in kidney of I/R induced mice after Pt/SAE treatment. The tubules were labeled with megalin (green). DAPI (blue) was used for nuclear staining. Scale bar = 40 μ m. **C, D** Flow cytometry showing the percentage of neutrophil (Ly6G +), M1 macrophage (iNOS +), M2 macrophage (CD206 +) infiltrated in the kidney of I/R induced mice after Pt/SAE treatment. $n = 5$. **G–I** Expression level of TNF α (**G**), IL-1 β (**H**) and IL-6 (**I**) production in kidneys were evaluated by ELISA. p -values are calculated using the Student's two-tailed t -test, * $p < 0.05$, ** $p < 0.01$, *** $p < 0.001$, **** $p < 0.0001$

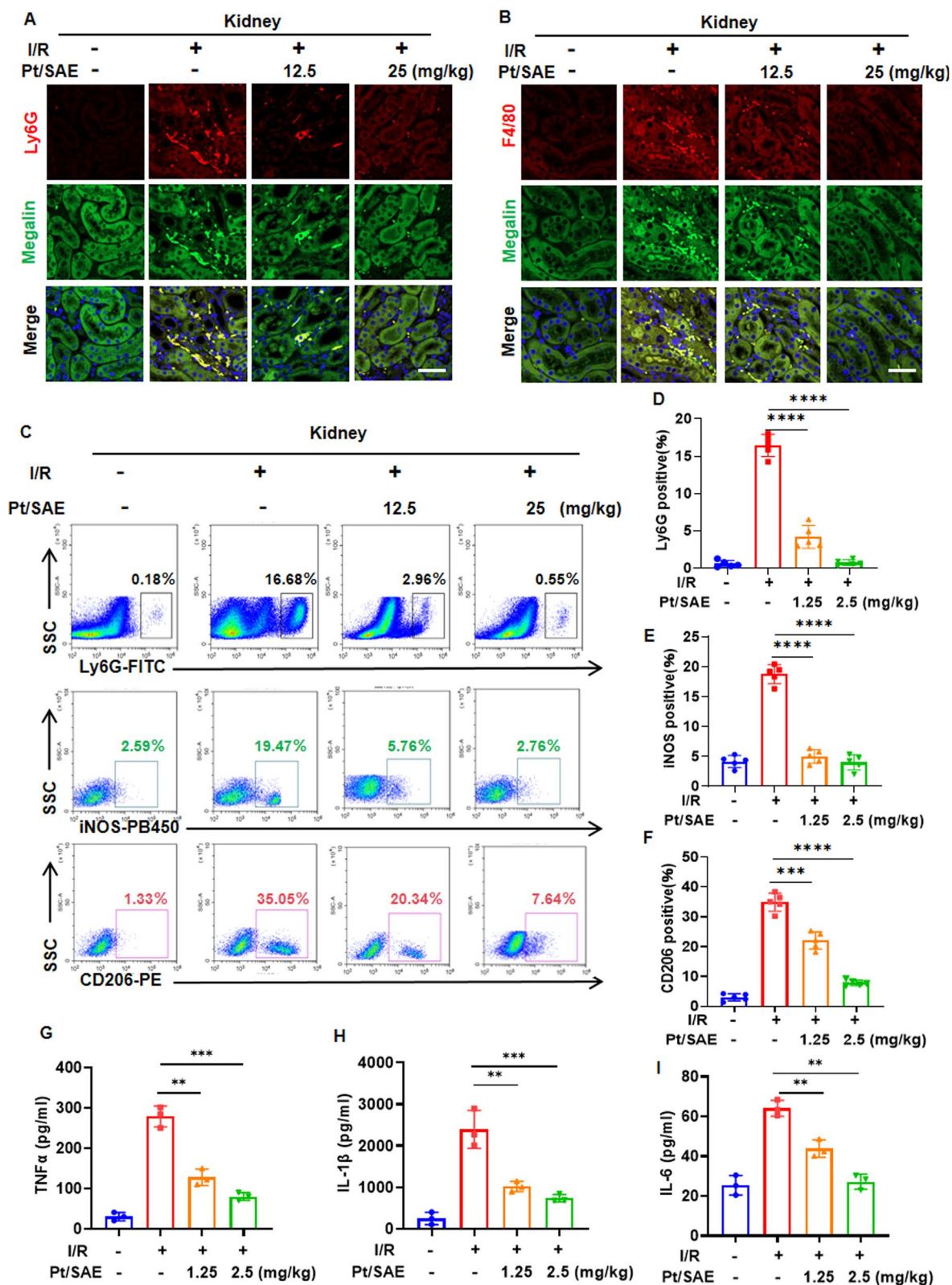


Fig. 8 (See legend on previous page.)

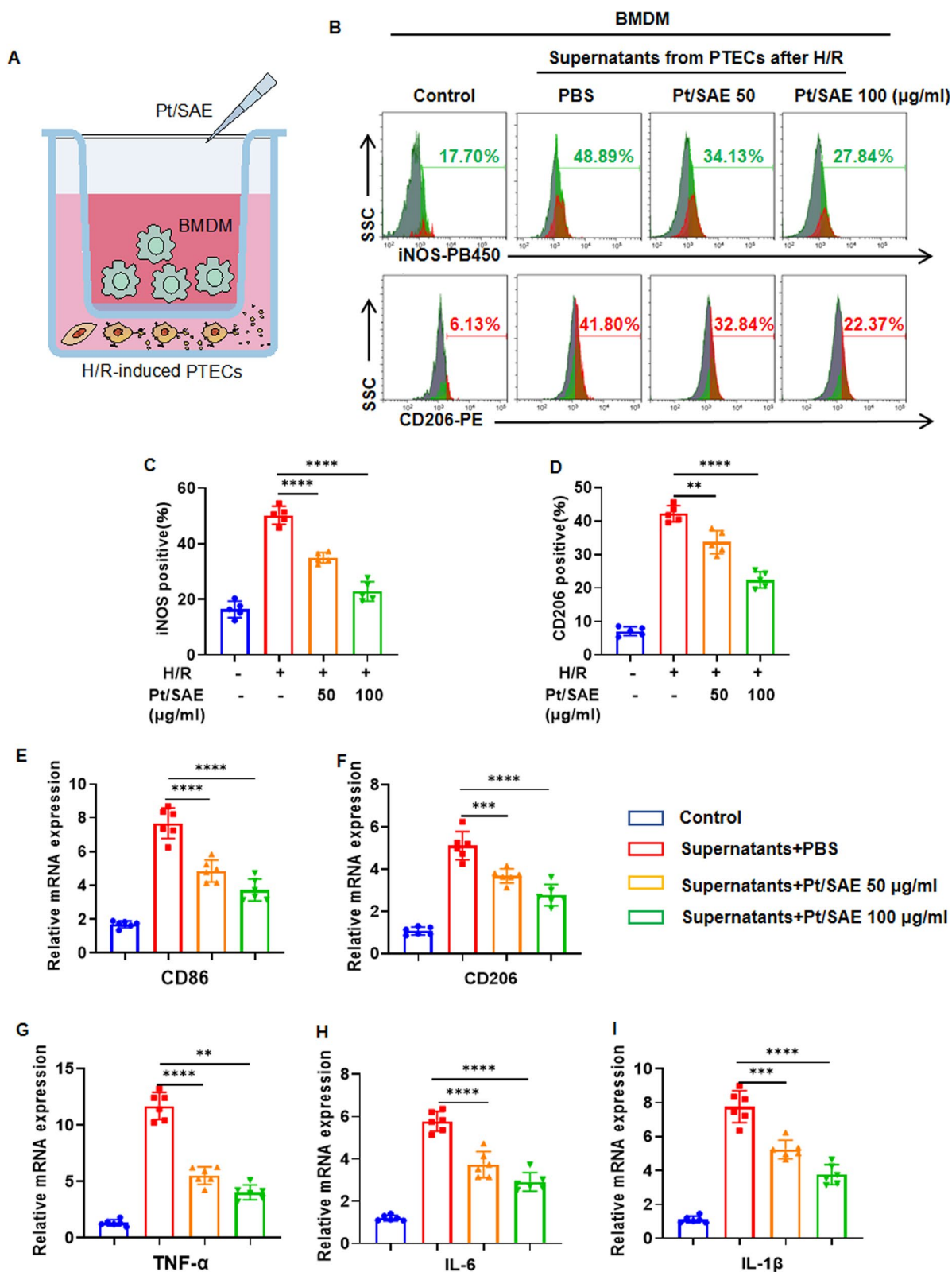


Fig. 9 Pt/SAE attenuates macrophages polarization induced by H/R in vitro. **A** Schematic diagram of the BMDM-H/R-stimulated PTECs co-culture system. **B–D** Flow cytometry revealed changes of BMDM polarization in different groups. $n = 5$. **E–J** Relative mRNA expression of CD86, CD206, TNF- α , IL-6 and IL-1 β in BMDMs determined by qPCR. $n = 5$. p -values are calculated using the Student's two-tailed t -test, $*p < 0.05$, $**p < 0.01$, $***p < 0.001$, $****p < 0.0001$

to clarify how IRI exosomes modulate ferroptosis [45–47]. Additionally, we observed that supernatants from necrotic PTECs induced by H/R enhanced macrophage polarization, suggesting that necrotic tubular cells drive immune cell inflammasome activation under IRI conditions. Recent studies have highlighted the role of mitochondrial reactive oxygen species (mtROS) in necroptosis and pyroptosis. During necroptosis, increased cellular reactive oxygen species (ROS) enhances RIPK1 phosphorylation and MLKL oligomerization, promoting necroptosis. Moreover, pyroptosis-mediated mtDNA release, driven by mtROS, triggers RIPK1/RIPK3/MLKL signaling and subsequent necroptosis. Our findings show that Pt/SAE effectively inhibits mtROS production, thereby suppressing cell death storm. However, the specific mechanisms linking mtROS to PANoptosis and ferroptosis require further investigation.

Advancements in nanotechnology, particularly targeted delivery systems, hold great promise for precise treatment of kidney diseases. Despite these developments, the application of nanotechnology in renal therapy remains in its early stages, and translating nanoparticles from animal models to clinical practice presents significant challenges.

Conclusion

This work demonstrates the effectiveness of a kidney-targeted and an antioxidant nanozyme with single-atomic Pt in alleviating I/R-induced cell death storm. The novel nanozyme not only exhibits significant antioxidant and iron-stress protective effects but also reduces inflammation and macrophages polarization, offering a promising new strategy for addressing acute kidney injury. Furthermore, the nanozyme has been shown to have minimal toxicity to kidney tissue, good biocompatibility, and safety, establishing a strong foundation for its potential clinical application. Overall, this research provides both theoretical and experimental support for the development of advanced nanomaterials aimed at improving the quality of life and treatment outcomes for acute kidney injury. However, further research is needed to explore its molecular mechanisms and clinical application to fully validate and support its use in clinical settings.

Supporting Information

Supporting Information is available from the Wiley Online Library or from the author.

Supplementary Information

The online version contains supplementary material available at <https://doi.org/10.1186/s12951-025-03392-0>.

Additional file 1.

Acknowledgements

No.

Author contributions

Y.X. and Y.Z. conceived and designed the experiments; K.Y. performed most of the experiments and wrote the initial draft of the manuscript; K.L. reviewed the manuscript; C.W. analyzed the data and drew the figures; Z. Zou. contributed to experiments; all authors reviewed and approved the final manuscript.

Funding

This work was supported by National Natural Science Foundation of China (U23 A20410), the Joint Funds for the innovation of science and Technology, Fujian province (2023Y9090 and 2021Y9100), Fujian Medical Innovation Project Funding Program (2024 CXA016), Young and Middle-aged Scientific Research Major Project of Fujian Provincial Health Commission (2021ZQNZD004).

Data availability

No datasets were generated or analysed during the current study.

Declarations

Ethics approval and consent to participate

Animal experiments were performed according to the protocol (IACUC FJMU 2023-Y-0719 and IACUC FJMU2022-0608) approved by the Ethical Committee of Fujian Medical University.

Competing interests

The authors declare no competing interests.

Author details

¹Department of Nephrology, Blood Purification Research Center, the First Affiliated Hospital, Fujian Medical University, Fuzhou 350005, Fujian, China. ²Research Center for Metabolic Chronic Kidney Disease, the First Affiliated Hospital, Fujian Medical University, Fuzhou 350005, Fujian, China. ³Department of Nephrology, National Regional Medical Center, Binhai Campus of the First Affiliated Hospital, Fujian Medical University, Fuzhou 350212, Fujian, China. ⁴School of Medicine, Nankai University, Tianjin 300071, China. ⁵Department of Neurosurgery, the First Affiliated Hospital, Fujian Medical University, Fuzhou 350005, China. ⁶Fujian Provincial Institutes of Brain Disorders and Brain Sciences, The First Affiliated Hospital, Fujian Medical University, Fuzhou 350005, China.

Received: 11 February 2025 Accepted: 15 April 2025

Published online: 27 April 2025

References

- Okusa MD, Rosner MH, Kellum JA, Ronco C. Therapeutic targets of human AKI: harmonizing human and animal AKI. *J Am Soc Nephrol*. 2016;27:44–8.
- Lin HYH, Chen Y, Chen Y-H, Ta AP, Lee H-C, MacGregor GR, Vaziri ND, Wang PH. Tubular mitochondrial AKT1 is activated during ischemia reperfusion injury and has a critical role in predisposition to chronic kidney disease. *Kidney Int*. 2021;99:870–84.
- Zeng X, McMahon GM, Brunelli SM, Bates DW, Waikar SS. Incidence, outcomes, and comparisons across definitions of AKI in hospitalized individuals. *Clin J Am Soc Nephrol*. 2014;9:12–20.
- Tanaka S, Tanaka T, Nangaku M. Hypoxia as a key player in the AKI-to-CKD transition. *Am J Physiol-Renal Physiol*. 2014;307:F1187–95.
- Su L, Zhang J, Gomez H, Kellum JA, Peng Z. Mitochondria ROS and mitophagy in acute kidney injury. *Autophagy*. 2023;19:401–14.
- Scholz H, Boivin FJ, Schmidt-Ott KM, Bachmann S, Eckardt K-U, Scholl UI, Persson PB. Kidney physiology and susceptibility to acute kidney injury: implications for renoprotection. *Nat Rev Nephrol*. 2021;17:335–49.
- Zhao M, Wang Y, Li L, Liu S, Wang C, Yuan Y, Yang G, Chen Y, Cheng J, Lu Y, Liu J. Mitochondrial ROS promote mitochondrial dysfunction and inflammation in ischemic acute kidney injury by disrupting TFAM-mediated mtDNA maintenance. *Theranostics*. 2021;11:1845–63.

8. Chen Q, Yang Y, Ying X, Huang C, Chen J, Wang J, Wu Z, Zeng W, Miao C, Shi X, et al. Hierarchical targeting nanodrug with holistic DNA protection for effective treatment of acute kidney injury. *Adv Sci*. 2025;2:2411254.
9. Liu M, Zhu Y, Jin D, Li L, Cheng J, Liu Y. Hemim-caged ferritin acting as a peroxidase-like nanozyme for the selective detection of tumor cells. *Inorg Chem*. 2021;60:14515–9.
10. Li L, Zhu Y, Liu M, Jin D, Zhang L, Cheng J, Liu Y. Conjugation of oxaliplatin with PEGylated-nanobody for enhancing tumor targeting and prolonging circulation. *J Inorg Biochem*. 2021;223:111553.
11. Chen Z, Li Y, Yuan Y, Lai K, Ye K, Lin Y, Lan R, Chen H, Xu Y. Single-cell sequencing reveals homogeneity and heterogeneity of the cytopathological mechanisms in different etiology-induced AKI. *Cell Death Dis*. 2023;14:318.
12. Zhu Y, Niu X, Wu T, Cheng J, Zou J, Pan Y, Tian Y, Huang W, Ding C, Lin Y, et al. Metal-phenolic nanocatalyst rewires metabolic vulnerability for catalytically amplified ferroptosis. *Chem Eng J*. 2024;485:150126.
13. Zhu Y, Ding C, Fang W, Li T, Yan L, Tian Y, Huang W, Wei P, Ma J, Lin X, et al. Metal-polyphenol self-assembled nanodots for NIR-II fluorescence imaging-guided chemodynamic/photodynamic therapy-amplified ferroptosis. *Acta Biomater*. 2024;185:361–70.
14. Wang L, Zhu Y, Zhang L, Guo L, Wang X, Pan Z, Jiang X, Wu F, He G. Mechanisms of PANoptosis and relevant small-molecule compounds for fighting diseases. *Cell Death Dis*. 2023;14:851.
15. Hou G, Chen Y, Lei H, Lu S, Cheng L. Nanomaterials-induced PANoptosis: a promising anti-tumor strategy. *Angew Chem Int Ed*. 2025;137:e202419649.
16. Jiang W, Hou X, Qi Y, Wang Z, Liu Y, Gao XJ, Wu T, Guo J, Fan K, Shang W. pH-activatable pre-nanozyme mediated H2S delivery for endogenous regulation of oxidative stress in acute kidney injury. *Adv Sci*. 2024;11:2303901.
17. Zhao X, Wang L-Y, Li J-M, Peng L-M, Tang C-Y, Zha X-J, Ke K, Yang M-B, Su B-H, Yang W. Redox-mediated artificial non-enzymatic antioxidant MXene nanoplateforms for acute kidney injury alleviation. *Adv Sci*. 2021;8:2101498.
18. Zhang DY, Tu T, Younis MR, Zhu KS, Liu H, Lei S, Qu J, Lin J, Huang P. Clinically translatable gold nanozymes with broad spectrum antioxidant and anti-inflammatory activity for alleviating acute kidney injury. *Theranostics*. 2021;11:9904–17.
19. Zheng J-J, Zhu F, Song N, Deng F, Chen Q, Chen C, He J, Gao X, Liang M. Optimizing the standardized assays for determining the catalytic activity and kinetics of peroxidase-like nanozymes. *Nat Protoc*. 2024;19:3470–88.
20. Song N, Yu Y, Zhang Y, Wang Z, Guo Z, Zhang J, Zhang C, Liang M. Bioinspired hierarchical self-assembled nanozyme for efficient antibacterial treatment. *Adv Mater*. 2024;36:2210455.
21. Huang W, Tian Y, Ma J, Wei P, Du C, Zhang X, Chen F, Lin Y, Zhu Y, Kang D. Neutrophil membrane-based biomimetic metal-polyphenol self-assembled nanozyme for the targeting treatment of early brain injury following subarachnoid hemorrhage. *Chem Eng J*. 2024;498:155643.
22. Rosenkrans ZT, Sun T, Jiang D, Chen W, Barnhart TE, Zhang Z, Ferreira CA, Wang X, Engle JW, Huang P, Cai W. Selenium-doped carbon quantum dots act as broad-spectrum antioxidants for acute kidney injury management. *Adv Sci*. 2020;7:2000420.
23. Cheng J, Pan Y, Zou J, Zhang M, Zhu Y, Liu Y, Chen X. Bioengineering nanomaterials for tumor therapy and anti-metastasis. *Prog Mater Sci*. 2025;148:101375.
24. Tang G, He J, Liu J, Yan X, Fan K. Nanozyme for tumor therapy: Surface modification matters. *Exploration*. 2021;1:75–89.
25. Huang Y, Ren J, Qu X. Nanozymes: classification, catalytic mechanisms, activity regulation, and applications. *Chem Rev*. 2019;119:4357–412.
26. Wu Q, Zhang J, Pan X, Huang Z, Zhang H, Guo J, Xue Y, Shi R, Liu H. Vacancy augmented piezo-sonosensitizer for cancer therapy. *Adv Sci*. 2023;10:2301152.
27. Zhang R, Jiang B, Fan K, Gao L, Yan X. Designing nanozymes for in vivo applications. *Nat Rev Biomed*. 2024;2:849–68.
28. Wu J, Wang X, Wang Q, Lou Z, Li S, Zhu Y, Qin L, Wei H. Nanomaterials with enzyme-like characteristics (nanozymes): next-generation artificial enzymes (II). *Chem Soc Rev*. 2019;48:1004–76.
29. Xu R, Zhang S, Wang P, Zhang R, Lin P, Wang Y, Gao L, Wei H, Zhang X, Ling D, et al. Nanozyme-based strategies for efficient theranostics of brain diseases. *Coord Chem Rev*. 2024;501:215519.
30. Chen M, Sun Y, Xu B, Yang Y, Wu Q, Lu M, Li F, Zhang J, Liu H. Photo-responsive nanozyme disrupts bacterial electron transport chain for enhanced anti-biofilm therapy. *Adv Funct Mater*. 2025;35:2417354.
31. Chen Q, Nan Y, Yang Y, Xiao Z, Liu M, Huang J, Xiang Y, Long X, Zhao T, Wang X, et al. Nanodrugs alleviate acute kidney injury: Manipulate RONS at kidney. *Bioact Mater*. 2023;22:141–67.
32. Wang K, Zhang Y, Mao W, Feng W, Lu S, Wan J, Song X, Chen Y, Peng B. Engineering ultrasmall ferroptosis-targeting and reactive oxygen/nitrogen species-scavenging nanozyme for alleviating acute kidney injury. *Adv Funct Mater*. 2022;32:2109221.
33. Tagaras N, Song H, Sahar S, Tong W, Mao Z, Buerki-Thurnherr T. Safety landscape of therapeutic nanozymes and future research directions. *Adv Sci*. 2024;11:2407816.
34. Li L, Liu X, Liu G, Xu S, Hu G, Wang L. Valence-engineered catalysis-selectivity regulation of molybdenum oxide nanozyme for acute kidney injury therapy and post-cure assessment. *Nat Commun*. 2024;15:8720.
35. Deng H, Qu Y, Chu B, Luo T, Pan M, Yuan L, Mo D, Bei Z, Yang T, Li X, et al. Macrophage membrane-biomimetic ROS-responsive platinum nanozyme clusters for acute kidney injury treatment. *Biomaterials*. 2025;317:123072.
36. Shan J, Du L, Wang X, Zhang S, Li Y, Xue S, Tang Q, Liu P. Ultrasound trigger Ce-based MOF nanoenzyme for efficient thrombolytic therapy. *Adv Sci*. 2024;11:2304441.
37. Mu X, Wang J, He H, Li Q, Yang B, Wang J, Liu H, Gao Y, Ouyang L, Sun S, et al. An oligomeric semiconducting nanozyme with ultrafast electron transfers alleviates acute brain injury. *Sci Adv*. 2021;7:eabk1210.
38. Zhu Y, Gong P, Wang J, Cheng J, Wang W, Cai H, Ao R, Huang H, Yu M, Lin L, Chen X. Amplification of lipid peroxidation by regulating cell membrane unsaturation to enhance chemodynamic therapy. *Angew Chem Int Ed*. 2023;62:e202218407.
39. Huang L, Chen J, Gan L, Wang J, Dong S. Single-atom nanozymes. *Sci Adv*. 2019;5:eaav5490.
40. Wang D, Wang J, Gao XJ, Ding H, Yang M, He Z, Xie J, Zhang Z, Huang H, Nie G, et al. Employing noble metal-porphyrins to engineer robust and highly active single-atom nanozymes for targeted catalytic therapy in nasopharyngeal carcinoma. *Adv Mater*. 2024;36:2310033.
41. Ma L, Zheng J-J, Zhou N, Zhang R, Fang L, Yang Y, Gao X, Chen C, Yan X, Fan K. A natural biogenic nanozyme for scavenging superoxide radicals. *Nat Commun*. 2024;15:233.
42. Ji S, Jiang B, Hao H, Chen Y, Dong J, Mao Y, Zhang Z, Gao R, Chen W, Zhang R, et al. Matching the kinetics of natural enzymes with a single-atom iron nanozyme. *Nat Catal*. 2021;4:407–17.
43. Linkermann A, Skouta R, Himmerkus N, Mulay SR, Dewitz C, De Zen F, Prokai A, Zuchtriegel G, Krombach F, Welz P-S, et al. Synchronized renal tubular cell death involves ferroptosis. *Proc Natl Acad Sci*. 2014;111:16836–41.
44. Li X, Peng X, Zhou X, Li M, Chen G, Shi W, Yu H, Zhang C, Li Y, Feng Z, et al. Small extracellular vesicles delivering lncRNA WAC-AS1 aggravate renal allograft ischemia-reperfusion injury by inducing ferroptosis propagation. *Cell Death Differ*. 2023;30:2167–86.
45. Zheng D-W, Pan P, Chen K-W, Fan J-X, Li C-X, Cheng H, Zhang X-Z. An orally delivered microbial cocktail for the removal of nitrogenous metabolic waste in animal models of kidney failure. *Nat Biomed Eng*. 2020;4:853–62.
46. Deng S, Cao H, Li T, Wang X, Meng J, Zeng T, Zhang D, Zhang S, Wang G, Liu R, et al. Lachnospiraceae-bacterium alleviates ischemia-reperfusion injury in steatotic donor liver by inhibiting ferroptosis via the Foxo3-Alox15 signaling pathway. *Gut Microbes*. 2025;17(1):2460543.
47. Yuan J, Yang M, Wu Z, Wu J, Zheng K, Wang J, Zeng Q, Chen M, Lv T, Shi Y, et al. The lactate-primed KAT8-PCK2 axis exacerbates hepatic ferroptosis during ischemia/reperfusion injury by reprogramming OXSM-dependent mitochondrial fatty acid synthesis. *Adv Sci*. 2025;24:e2414141.

Publisher's Note

Springer Nature remains neutral with regard to jurisdictional claims in published maps and institutional affiliations.